Food Chemistry: X 13 (2022) 100211

Contents lists available at ScienceDirect

Food Chemistry: X

journal homepage: www.sciencedirect.com/journal/food-chemistry-x

Preparation, chemical structure, and immunostimulatory activity of a water-soluble heteropolysaccharide from *Suillus granulatus* fruiting bodies

Xiong Gao [a], Ranhua Zeng [c], Chi-Tang Ho [d], Bin Li [c,e], Shaodan Chen [a], Chun Xiao [a], Huiping Hu [a], Manjun Cai [a], Zhongzheng Chen [c,e], Yizhen Xie [a,b,*], Qingping Wu [a,*]

[a] *State Key Laboratory of Applied Microbiology Southern China, Guangdong Provincial Key Laboratory of Microbial Safety and Health, Institute of Microbiology, Guangdong Academy of Sciences, Guangzhou 510070, China*
[b] *Guangdong Yuewei Biotechnology Co. Ltd., Zhaoqing 526000, China*
[c] *College of Food Science, South China Agricultural University, 483 Wushan Street, Tianhe District, Guangzhou 510642, China*
[d] *Department of Food Science, Rutgers University, 65 Dudley Road, New Brunswick, NJ 08901, USA*
[e] *Guangdong Provincial Key Laboratory of Nutraceuticals and Functional Foods, South China Agricultural University, Guangzhou 510642, China*

ARTICLE INFO

Keywords:
Suillus granulatus
Heteropolysaccharide
Structural characterization
Immunomodulatory activity

ABSTRACT

A water-soluble heteropolysaccharide (SGP2-1) was purified from *Suillus granulatus* fruiting bodies by anion-exchange chromatography and gel permeation chromatography. The structural characteristics were analyzed by high-performance gel permeation chromatography, high-performance liquid chromatography, Fourier transform infrared spectroscopy, gas chromatography-mass spectrometry, and nuclear magnetic resonance spectroscopy. The immunostimulatory activity was investigated using RAW 264.7 macrophages. Results showed that SGP2-1 with weight average molecular weight of 150.75 kDa was composed of mannose, glucose, and xylose. The backbone of SGP2-1 was mainly composed of → 4)-*α*-Glc*p*-(1→, and the terminal group *α*-D-Glc*p* → was linked to the main chain by *O*-6 position. SGP2-1 could significantly enhance pinocytic capacity, reactive oxygen species production, and cytokines secretion. SGP2-1 exerted immunomodulatory effects through interacting with toll-like receptor 2, and activating mitogen-activated protein kinase, phosphatidylinositol-3-kinase/protein kinase B, and nuclear factor-kappa B signaling pathways. These findings indicated that SGP2-1 could be explored as a potential immunomodulatory agent for application in functional foods.

1. Introduction

Natural polysaccharides have received increasing attention due to their low toxicity and diverse health-promoting effects such as immunomodulatory (Liu, Amakye, & Ren, 2021), antioxidant (Teng et al., 2021), anti-photoaging (Yao et al., 2021), and anti-tumor activities (Li, You, Dong, Yao, & Chen, 2020). Mushrooms have a long history of medicinal applications and their polysaccharides have been considered as major bioactive components. The innate immune system is the first line of host defense against infections, pollutants, and pathogens (Rungelrath, Kobayashi, & DeLeo, 2020). In recent decades, extensive studies have demonstrated that mushroom polysaccharides exert remarkable immunostimulating effects. They improve immune function through activating host immune cells such as macrophages (Ren et al., 2019), dendritic cells (Liu, Choi, Xue & Cheung, 2019), and natural killer cells (Lemieszek, Nunes, & Rzeski, 2019). As examples, the polysaccharides

Abbreviations: NO, Nitric oxide; HPGPC, High-performance gel permeation chromatography; GC-MS, Gas chromatography-mass spectrometry; FT-IR, Fourier transform infrared spectroscopy; NMR, Nuclear magnetic resonance; LPS, Lipopolysaccharides; D_2O, Deuterium oxide; DCFH-DA, 2′,7′-Dichlorofluorescein diacetate; PMP, 1-Phenyl-3-methyl-5-pyrazolone; TNF-α, Tumor necrosis factor-α; MCP-1, Monocyte chemoattractant protein-1; IL-6, Interleukin-6; ELISA, Enzyme-linked immunosorbent assay; RIPA, Radioimmunoprecipitation assay; DMEM, Dulbecco's modified Eagle's medium; DPBS, Dulbecco's phosphate-buffered saline; CCK-8, Cell counting kit-8; ERK, Extracellular signal-regulated kinase; Akt, Protein kinase B; NF-κB, Nuclear factor-kappa B; JNK, c-Jun *N*-terminal kinase; IκBα, I kappa B alpha; PI3K, Phosphatidylinositol-3-kinase; TLR4, Toll-like receptor 4; TLR2, Toll-like receptor 2; HPLC, High performance liquid chromatography; ROS, Reactive oxygen species; RT-PCR, Reverse transcription-polymerase chain reaction; iNOS, Inducible nitric oxide synthase; ANOVA, Analysis of variance; Mw, Weight average molecular weight; DEPT, Distortionless enhancement by polarization transfer; ^{1}H-^{1}H COSY, ^{1}H-^{1}H correlation spectroscopy; HSQC, Heteronuclear single quantum correlation; HMBC, Heteronuclear multiple bond correlation; MAPKs, Mitogen-activated protein kinase.

* Corresponding authors.
E-mail addresses: xieyz@gdim.cn (Y. Xie), wuqp203@163.com (Q. Wu).

https://doi.org/10.1016/j.fochx.2022.100211
Received 15 September 2021; Received in revised form 10 January 2022; Accepted 12 January 2022
Available online 15 January 2022

from *Ganoderma leucocontextum* exhibited immunoregulatory activity through promoting the production of nitric oxide (NO), cytokines, and chemokines from macrophages *in vitro* (Gao et al., 2020). A water-soluble polysaccharide from *Hericium erinaceus* could significantly ameliorate the immunosuppression in cyclophosphamide-treated mice by enhancing splenocyte proliferation, natural killer cell activity, and macrophage phagocytosis (Wu & Huang, 2021). Therefore, some mushroom polysaccharides have been used in functional food and pharmaceutical industries (Ren, Zhang, & Zhang, 2021).

Suillus granulatus, which belongs to Eumycota Basidiomycetes, is a wild edible mushroom available in China and other countries. Because of its rich nutrients and unique flavor, *S. granulatus* is very popular among consumers (Zhao, Wei, Gong, Xu, & Xin, 2020). It has been found that *S. granulatus* possesses a variety of active ingredients and health benefits (Reis et al., 2014; Ribeiro et al., 2008). To the best of our knowledge, the chemical structure and biological activity of *S. granulatus* polysaccharides have not been well-documented. Only Chen, Su, and Wang (2018) reported that two polysaccharide fractions from *S. granulatus* fruiting bodies had antioxidant activity and could promote lymphocyte proliferation *in vitro*. However, the structural information of *S. granulatus* polysaccharides is still needed to be further elucidated, and the immunoregulatory mechanism remains unclear.

In the current study, a new polysaccharide fraction, designated SGP2-1, was separated from *S. granulatus*. The chemical structure of SGP2-1 was characterized by high-performance gel permeation chromatography (HPGPC), gas chromatography-mass spectrometry (GC-MS), Fourier transform infrared spectroscopy (FT-IR), and nuclear magnetic resonance spectroscopy (NMR). In addition, the immunostimulatory activity *in vitro* of SGP2-1 and its underlying mechanism were evaluated by using RAW 264.7 murine macrophages. Knowledge obtained from this study is of importance for understanding the structure and immunoregulatory activities of *S. granulatus* polysaccharides.

2. Materials and methods

2.1. Materials

RAW 264.7 cell line was obtained from the American Type Culture Collection (Manassas, VA, USA). *S. granulatus* fruiting bodies were purchased from Beiyuzhenqi Forest Food Co., Ltd. (Ning'an, China), and the species was identified by the senior engineer Huiping Hu (Guangdong Institute of Microbiology, Guangzhou, China). Lipopolysaccharides (LPS), deuterium oxide (D_2O), 2′,7′-dichlorofluorescein diacetate (DCFH-DA), 1-phenyl-3-methyl-5-pyrazolone (PMP), dextran standards (5.2, 11.6, 23.8, 48.6, 148, 273, 410, 668 kDa), and neutral red were purchased from Sigma (St. Louis, USA). Monosaccharide standards were obtained from Bo Rui Saccharide Biotech Co., Ltd. (Yangzhou, China). Tumor necrosis factor-α (TNF-α), monocyte chemoattractant protein-1 (MCP-1), and interleukin-6 (IL-6) enzyme-linked immunosorbent assay (ELISA) kits were obtained from NeoBioScience Technology Co., Ltd. (Shenzhen, China). NE-PER nuclear and cytoplasmic extraction reagents, radioimmunoprecipitation assay (RIPA) buffer, NuPAGE Bis-Tris gels, Dulbecco's modified Eagle's medium (DMEM), Dulbecco's phosphate-buffered saline (DPBS), and TRIzol reagent were purchased from Thermo Scientific (Rockford, USA). SP600125, U0126, SB203580, LY294002, BAY 11-7082, and cell counting kit-8 (CCK-8) were obtained from MedChemExpress (Monmouth Junction, USA). The antibodies against extracellular signal-regulated kinase (ERK), p-ERK, and protein kinase B (Akt) were obtained from Affinity Biosciences (Cincinnati, USA). The antibodies against nuclear factor-kappa B (NF-κB) p65, p-NF-κB p65, c-Jun *N*-terminal kinase (JNK), p-JNK, p38, p-p38, I kappa B alpha (IκBα), p-IκBα, phosphatidylinositol-3-kinase (PI3K) p85, p-Akt, GAPDH, and Lamin B1 were obtained from Cell Signaling Technology (Boston, USA). The antibodies against toll-like receptor 4 (TLR4), toll-like receptor 2 (TLR2), and p-PI3K p85 were obtained from Abcam (Cambridge, UK). The endotoxin removal kit was purchased from Yeasen Biotech Co., Ltd. (Shanghai, China).

2.2. Extraction and purification of polysaccharides

Ground fruiting bodies of *S. granulatus* were defatted by pretreating twice with 95% ethanol (75 °C, 2 h) in a 1:20 solid–liquid ratio (w/v). After filtration, the defatted residue was dried at 60 °C. The dried residue was extracted with distilled water (90 °C) 3 times in a 1:20 solid–liquid ratio (w/v) for 2 h. The extraction solutions were concentrated and mixed with ethanol (final concentration 30%) at 4 °C for 3 h to precipitate insoluble polysaccharides (Yi et al., 2019). After centrifugation, the ethanol concentration in the supernatant was increased to 80% (4 °C, 16 h). The precipitate was collected by centrifugation and deproteinized using Sevag reagent (Shi, Zhong, Zhang, & Yan, 2020). The aqueous phase was dialyzed against ultrapure water (cut-off Mw 3.5 kDa) and then lyophilized to obtain crude *S. granulatus* polysaccharides (CSGP).

The CSGP (150 mg) was redissolved in 6 mL ultrapure water and subjected to a DEAE-Sepharose fast flow column (2.6 × 30 cm). The column was eluted with ultrapure water and different concentration of NaCl solutions (0.1–1.0 M, 2 mL/min). The eluates (8 mL/tube) were collected, and the total carbohydrate content was sequentially detected using the phenol–sulfuric acid method. Three sections (SGP1, SGP2, and SGP3) were obtained, dialyzed and freeze-dried. SGP2 fraction, which had the highest yield, was further purified using a Sephacryl S-300 HR column (2.6 × 60 cm). NaCl solution (0.1 M, 1 mL/min) was applied to elute the column. The major eluted fraction was dialyzed, lyophilized, and named as SGP2-1.

2.3. Component analysis and molecular weight determination

The contents of the total carbohydrates and proteins were determined according to our previous method (Gao et al., 2020). The molecular weight of SGP2-1 was measured by HPGPC. The polysaccharide sample was eluted with $NaNO_3$ (0.1 M, 0.4 mL/min), and the column was calibrated by dextran standards.

2.4. Monosaccharide composition analysis

Monosaccharide composition of SGP2-1 was performed on high performance liquid chromatography (HPLC) as described by a previous study (Niu et al., 2014). Briefly, SGP2-1 (2 mg) was mixed with 1 mL of 2 M trifluoroacetic acid and hydrolyzed at 110 °C for 6 h. The solution was cooled, and the excess trifluoroacetic acid was removed through multiple co-evaporation with methanol. The residue was dissolved in ultrapure water (200 μL) and then added with 0.3 M NaOH (100 μL). Subsequently, the derivatization was conducted by adding 0.5 M PMP (100 μL) at 70 °C for 100 min. The resulting solution was neutralized by 0.3 M HCl (100 μL), and then 0.5 mL of chloroform was added. After centrifugation (3000 rpm, 10 min, 15 °C), the aqueous phase was detected by an Agilent 1200 Series HPLC system equipped with an Eclipse XDB-C18 column. The mobile phase was mixed with 84% PBS (0.1 M, pH 6.5) and 16% acetonitrile. The detection wavelength, column temperature, and flow rate were set to 250 nm, 30 °C, and 0.8 mL/min, respectively. The monosaccharide standards were processed with the same procedure.

2.5. FT-IR, methylation, and NMR analysis

The FT-IR spectrum of SGP2-1 from 400 cm^{-1} to 4000 cm^{-1} was analyzed by the potassium bromide disk method using a Bruker Vertex 70 spectrometer.

Methylation analysis of SGP2-1 was analyzed as described by a previous method (Chen, Zhu, Ma, Zhang, & Wu, 2019).

SGP2-1 (50 mg) was redissolved in D_2O at a concentration of 100 mg/mL after exchange with D_2O two times. The 1D and 2D NMR spectra

of SGP2-1 were obtained by using the Bruker AVANCE III 600 MHz apparatus.

2.6. Immunomodulatory activity of SGP2-1

2.6.1. Cell viability

To avoid endotoxin contamination in immunoregulatory experiments, the potential endotoxin in SGP2-1 was removed by using endotoxin removal kit. RAW 264.7 cells (5×10^5 cells/mL) were seeded on a 96-well plate and treated with various concentrations of SGP2-1 (40, 80, 160, and 320 μg/mL) for 24 h. Afterward, CCK-8 solution (200 μL) diluted in serum-free DMEM was added to each well, and the absorbance was recorded at 450 nm.

2.6.2. Pinocytic activity

The pinocytic capacity was evaluated according to the neutral red staining method. Briefly, RAW 264.7 cells (5×10^5 cells/mL) were seeded on a 96-well microplate incubated with different concentrations of SGP2-1 (40, 80, 160, and 320 μg/mL) or LPS (100 ng/mL) for 24 h. Subsequently, the medium was replaced with 0.1% neutral red (100 μL), and the plate was further incubated for 1 h. Finally, the cells were lysed with 100 μL of cell lysates (ethanol and acetic acid mixed in equal volume) after washing with DPBS three times. The absorbance was recorded at 540 nm.

2.6.3. Measurement of intracellular reactive oxygen species (ROS)

DCFH-DA fluorescence probe was used to determine the intracellular ROS level as described by a previous study (Ren, Lin, Alim, Zheng, & Yang, 2017). RAW 264.7 cells (5×10^5 cells/mL) were seeded on a 6-well plate. After treatment with various concentrations of SGP2-1 or LPS (100 ng/mL) for 24 h, cells were stained with DCFH-DA solution (10 μM) in dark for 30 min. Finally, CytoFLEX flow cytometer and Axio Observer A1 fluorescence microscope were applied to analyze the intracellular ROS level.

2.6.4. Measurement of NO, TNF-α, IL-6, and MCP-1

RAW 264.7 cells (5×10^5 cells/mL) were treated with different concentrations of SGP2-1 or LPS (100 ng/mL) for 24 h. Then the cell culture supernatants were collected. The NO, IL-6, TNF-α, and MCP-1 levels were measured by Griess reagent and commercial ELISA kits.

The effects of signal transduction pathways on SGP2-1-induced macrophage activation were further investigated. RAW 264.7 cells (5×10^5 cells/mL) were pretreated with SP600125 (30 μM), U0126 (30 μM), SB203580 (30 μM), LY294002 (30 μM), and BAY 11-7082 (10 μM) for 1 h and then co-cultured with SGP2-1 (320 μg/mL). After 24 h treatment, the NO, TNF-α, and IL-6 levels were determined as described above.

2.6.5. RNA extraction and reverse transcription-polymerase chain reaction (RT-PCR)

RAW 264.7 cells (5×10^5 cells/mL) were treated with different concentrations of SGP2-1 or LPS (100 ng/mL) for 24 h. Then TRIzol reagent was used to extract total RNA. cDNA Synthesis Kit (Servicebio Technology Co., Ltd., Wuhan, China) was used to reverse-transcribe cellular RNA into cDNA. All primers were listed as follows: β-Actin, F: 5′-CCACCATGTACCCAGGCATT-3′ and R: 5′-CAGCTCAGTAACAGTCCGCC-3′; Inducible nitric oxide synthase (iNOS), F: 5′-CCTCACGCTTGGGTCTTGTT-3′ and R: 5′-TGAGAACAGCACAAGGGGTTT-3′; MCP-1, F: 5′-GCAGGTCCCTGTCATGCTTCT-3′ and R: 5′-TGTCTGGACCCATTCCTTCTTG-3′; TNF-α, F: 5′-AAGTTCCCAAATGGCCTCCC-3′ and R: 5′-TTGCTACGACGTGGGCTAC-3′; IL-6, F: 5′-CCCCAATTTCCAATGCTCTCC-3′ and R: 5′-CGCACTAGGTTTGCCGAGTA-3′. Quantitative real-time RT-PCR was performed on a CFX Connect system using SYBR Green qPCR Master Mix (Servicebio Technology Co., Ltd.). The relative mRNA expression level was analyzed by the $2^{-\Delta\Delta Ct}$ method.

2.6.6. Toll-like receptors blocking experiment

RAW 264.7 cells (5×10^5 cells/mL) were pretreated with 10 μg/mL of anti-TLR2, anti-TLR4, or anti-TLR2 + anti-TLR4 for 1 h before treatment with SGP2-1 (320 μg/mL). After 24 h incubation, the NO and IL-6 levels were determined as described in Section 2.6.4.

2.6.7. Western blot analysis

After treatment with different concentrations of SGP2-1 or LPS (100 ng/mL) for 30 min, RIPA buffer added with phosphatase and protease inhibitors (ApexBio Technology, Houston, TX, USA) was used to extract the whole cellular proteins. In addition, NE-PER nuclear and cytoplasmic kit was used to extract the cellular nuclear and cytoplasmic proteins. The extracted proteins were separated on NuPAGE Bis-Tris gels and transferred to a polyvinylidene fluoride membrane (Millipore, Billerica, USA). Next, the membrane was blocked with 5% non-fat milk and incubated at 4 °C overnight with primary antibodies. Finally, the membrane was incubated with secondary antibody. The protein band was visualized via enhanced chemiluminescence reagent on an Omega Lum G imaging system.

2.7. Statistical analysis

The data were analyzed by SAS v9.2 software (Cary, USA) and expressed as mean ± standard deviation. Duncan's multiple-range test and one-way analysis of variance (ANOVA) were used to evaluate significant differences between the groups. $p < 0.05$ was considered to be statistically significant.

3. Results and discussion

3.1. Extraction and purification

The CSGP was extracted from *S. granulatus* fruiting bodies in a yield of 1.69% by hot-water extraction, ethanol precipitation, and deproteination. Sequentially, CSGP was subjected to DEAE-Sepharose fast flow, and three fractions (SGP1, SGP2, and SGP3) were obtained (Fig. 1A). The yields of SGP1, SGP2, and SGP3 were 0.15%, 0.47%, and 0.20%, respectively. In the present study, Sephacryl S-300 HR was used to further purify SGP2 fraction due to its highest yield (Fig. 1B). The main peak SGP2-1 with a yield of 0.27% was obtained and its total carbohydrate content was 94.84%. In addition, no absorption at 260 nm and 280 nm were found in the UV–visible spectrum of SGP2-1, suggesting that the absence of nucleic acids or proteins (Fig. 1C). The protein content of SGP2-1 was only 0.08%, which was supported by the result of UV–visible spectrum.

3.2. Molecular weight and monosaccharide composition

A single and symmetrical peak was observed in the HPGPC chromatogram, implying that SGP2-1 was a homogeneous polysaccharide (Fig. 1D). The weight average molecular weight (Mw) of SGP2-1 was estimated to be 150.75 kDa. The monosaccharide composition analysis of SGP2-1 is shown in Fig. 1E. SGP2-1 was composed of mannose, glucose, and xylose in a molar ratio of 7.6: 89.2: 3.2. The result indicated that SGP2-1 was a heteropolysaccharide with high glucose content.

3.3. FT-IR spectroscopy

The FT-IR spectrum of SGP2-1 is shown in Fig. 1F. The characteristic peaks at 3379.14 and 2929.28 cm^{-1} were the stretching vibrations of O—H and C—H, respectively (Yu et al., 2019). The band at 1647.36 cm^{-1} was probably assigned to the associated water (Wang, Yin, Huang, & Nie, 2020). The bands at 1417.28 and 1367.14 cm^{-1} were assigned to the bending vibrations of CH_2 and CH, respectively (Ren, Zhao, Zheng, Alim, & Yang, 2019; Wu, Zhou, Zhou, Ou, & Huang, 2017). The intense bands at 1155.00, 1080.28, and 1024.36 cm^{-1} implied the presence of

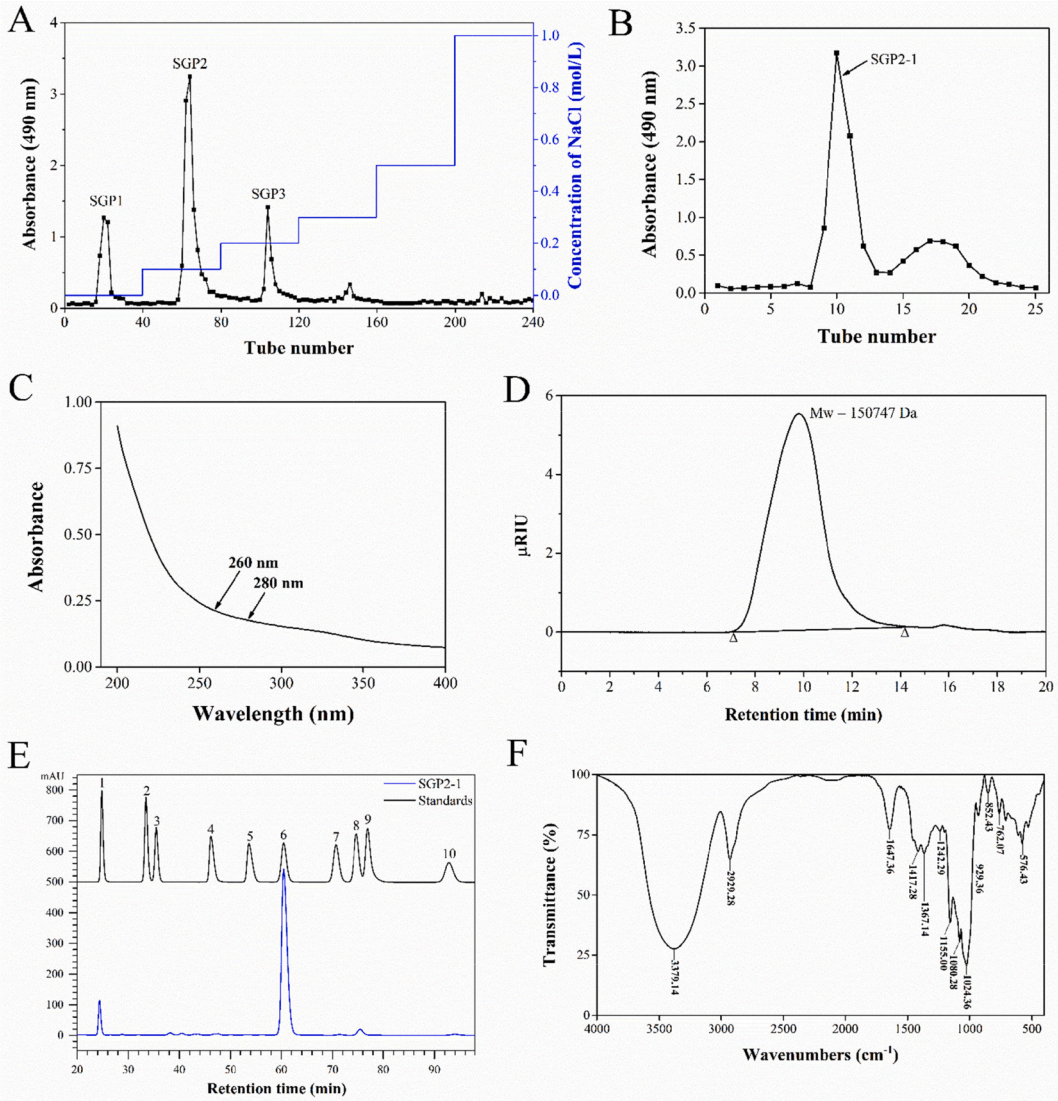

Fig. 1. Stepwise elution profile of SGP2-1 on a DEAE-Sepharose fast flow column (A); Elution profile of SGP2 on a Sephacryl S-300 HR column (B); UV–visible spectrum of SGP2-1 (C); HPGPC chromatogram of SGP2-1 (D); Monosaccharide composition of SGP2-1 analyzed by HPLC (1-mannose, 2-ribose, 3-rhamnose, 4-glucuronic acid, 5-galacturonic acid, 6-glucose, 7-galactose, 8-xylose, 9-arabinose, and 10-fucose) (E); FT-IR spectrum of SGP2-1 (F).

pyran-glycosides (Cheng et al., 2017). The peak at 929.36 cm^{-1} was ascribed to the asymmetric stretching vibration of pyranose ring (Teng et al., 2021). Both bands at 852.43 and 762.07 cm^{-1} were assigned to the symmetrical stretching vibrations of α-isomeric pyranose (Cheng et al., 2017). In addition, the bands at 576.43 cm^{-1} also suggested that SGP2-1 contained the pyranose residue (Shi et al., 2020).

3.4. Methylation analysis

To elucidate the types of glycosidic linkages, the methylation of SGP2-1 was identified by GC-MS. According to the literatures as well as mass spectral analysis (Tabarsa et al., 2020; Teng et al., 2021; Zheng et al., 2020), the linkage types in SGP2-1 are shown in Table 1 and Fig. S1. SGP2-1 contained six glycosidic bonds: 2,3,4-Me_3-Xyl*p*, 2,3,4,6-Me_4-Glc*p*, 2,3,6-Me_3-Glc*p*, 2,4,6-Me_3-Man*p*, 4,6-Me_2-Man*p*, and 2,3-Me_2-Glc*p*. The dominant residues including Glc*p*-(1→, →4)-Glc*p*-(1→, and → 4,6)-Glc*p*-(1 → accounted for 17.7%, 58.8%, and 11.6%, respectively. Additionally, a small amount of Xyl*p*-(1→ (2.6%), →3)-Man*p*-(1→ (6.4%), and → 2,3)-Man*p*-(1→ (2.9%) residues were also found. This result is consistent with the monosaccharide composition analysis.

Table 1
Methylation analysis of SGP2-1 by GC-MS.

Methylated sugar	Linkage pattern	Molar ratios	Mass fragments (*m/z*)
2,3,4-Me_3-Xyl*p*	*T*-Xyl*p*-(1→	2.6	43,71,87,101,117,129,131,161
2,3,4,6-Me_4-Glc*p*	*T*-Glc*p*-(1→	17.7	43,71,87,101,117,129,145,161,205
2,3,6-Me_3-Glc*p*	→4)-Glc*p*-(1→	58.8	43,87,99,101,113,117,129,131,161,173,233
2,4,6-Me_3-Man*p*	→3)-Man*p*-(1→	6.4	43,71,85,87,99,101,117,129,161,201,233
4,6-Me_2-Man*p*	→2,3)-Man*p*-(1→	2.9	43,85,87,99,101,127,129,161,201,261
2,3-Me_2-Glc*p*	→4,6)-Glc*p*-(1→	11.6	43,71,85,87,99,101,117,127,159,161,201

3.5. NMR spectra

The chemical structure of SGP2-1 was further elucidated by NMR spectroscopy. According to previous literatures (Cao et al., 2020; Teng et al., 2021; Wang et al., 2017; Xie et al., 2020; Zhai et al., 2021), all the carbon and proton signals were assigned and presented in Table S1. The signals at 101.05, 99.88, 101.33, 104.81, 103.96, and 103.35 ppm in the ^{13}C NMR spectrum were assigned to C1 of **A**, **B**, **C**, **D**, **E**, and **F**, respectively (Fig. 2A). No significant peaks at 170–180 ppm suggested that SGP2-1 contained a very low content of uronic acid. The signals at 5.31, 4.89, 5.26, and 4.36 ppm in the ^{1}H NMR spectrum corresponded with H1 of **A**, **B**, **C**, and **D**, respectively (Fig. 2B). Additionally, the distortionless enhancement by polarization transfer (DEPT)-135 spectrum revealed the C6 chemical shifts of sugar residue (Fig. S2).

All the C/H chemical shifts of SGP2-1 were further assigned by 2D NMR spectra. Residue **A** (→4)-*α*-Glc*p*-(1 →) was taken as an example. An anomeric proton signal at 5.31 ppm was detected. Two cross-peaks at 5.31/3.55 and 3.55/3.90 ppm were obtained from ^{1}H-^{1}H correlation spectroscopy (^{1}H-^{1}H COSY) spectrum (Fig. 2C). It indicated that 3.55 and 3.90 ppm corresponded with H2 and H3, respectively. The typical H4 (3.58 ppm), H5 (3.78 ppm), and H6 (3.79 ppm) showed intra-correlations in the ^{1}H-^{1}H COSY spectrum. From the heteronuclear single quantum correlation (HSQC) spectrum (Fig. 2D), a strong signal of H1/C1 (5.31/101.05 ppm) in the anomeric region suggested that H1 exhibited close connectivity with C1. Additionally, the carbon peaks of *C*2 (72.91 ppm), C3 (74.56 ppm), C4 (78.31 ppm), C5 (72.53 ppm), and C6 (61.89 ppm) were also observed. These values were corresponded closely with previous study (Xie et al., 2020). The assignments of other residues were conducted following the same procedure.

The heteronuclear multiple bond correlation (HMBC) spectrum was

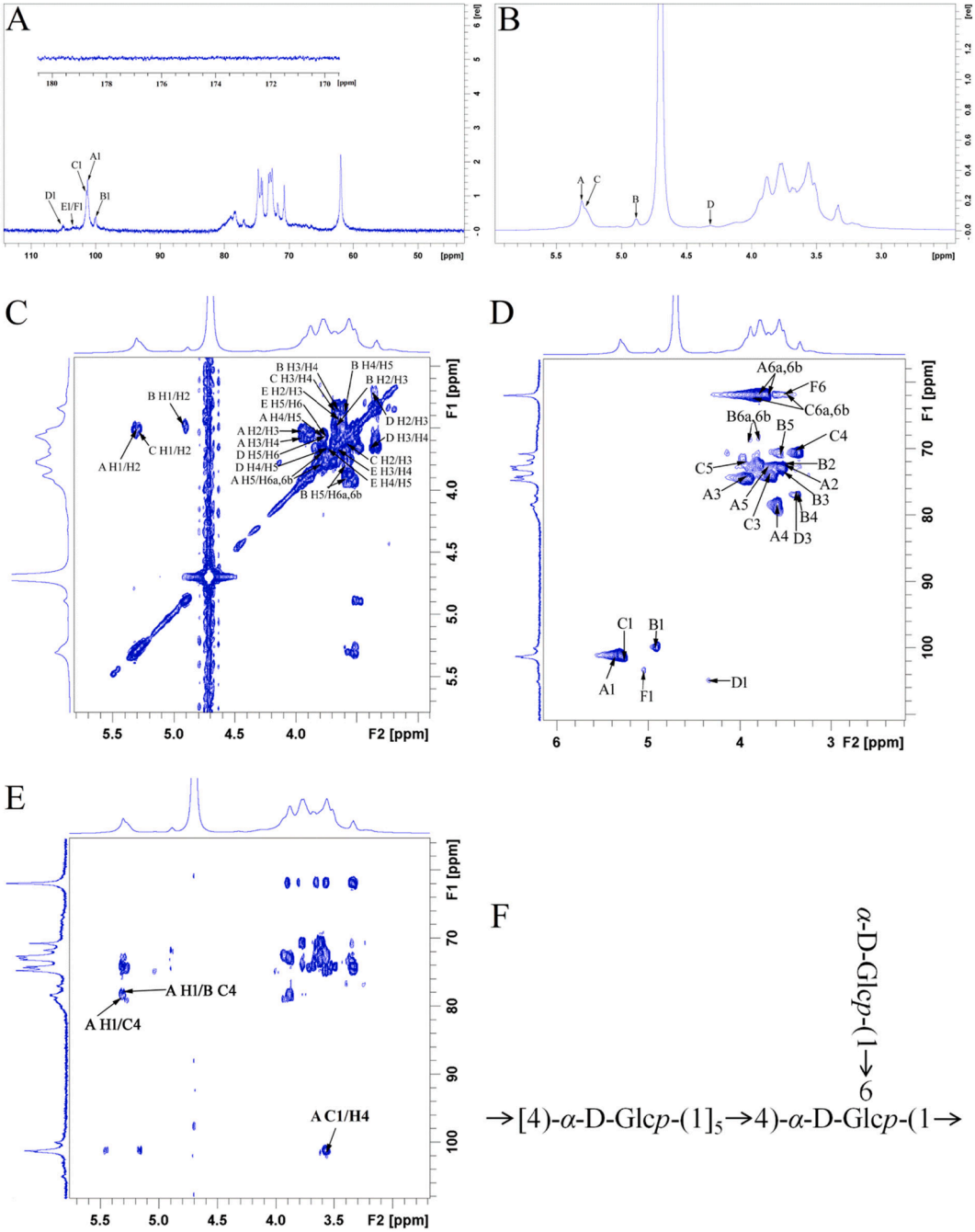

Fig. 2. ^{13}C NMR (A), ^{1}H NMR (B), ^{1}H–^{1}H COSY (C), HSQC (D), and HMBC (E) spectra of SGP2-1, and the main backbone of SGP2-1 (F).

conducted to figure out the linkage sequences of SGP2-1 (Fig. 2E). The cross-peaks **A** C1/H4, **A** H1/C4, and **A** H1/**B** C4 suggested that the presence of → 4)-*α*-Glc*p*-(1 → 4)-*α*-Glc*p*-(1 → 4,6)-*α*-D-Glc*p*-(1→. Based on the monosaccharide composition, methylation, and NMR data, it could be concluded that the backbone of SGP2-1 was mainly composed of → 4)-*α*-Glc*p*-(1→. The terminal group *α*-D-Glc*p* → was linked to the main chain via *O*-6 position of glucose (Fig. 2F). Additionally, the result of methylation analysis showed that SGP2-1 also contained Xyl*p*-(1→, →3)-Man*p*-(1→, and → 2,3)-Man*p*-(1 → residue. However, no obvious linkages of these residues could be obtained from the HMBC spectrum, which was partly attributed to their low content.

3.6. Immunomodulatory effects of SGP2-1 on RAW 264.7 cells

3.6.1. SGP2-1 promoted cell proliferation

In this study, RAW 264.7 macrophages were applied to evaluate the immunoregulatory activities of SGP2-1. RAW 264.7 macrophages were treated with SGP2-1 (40, 80, 160, and 320 μg/mL), and the viability was determined by the CCK-8 assay. Compared with the untreated group, SGP2-1 notably promoted RAW 264.7 cells proliferation (Fig. 3A). The result suggested that SGP2-1 showed no cytotoxic effects in the concentration range.

3.6.2. SGP2-1 enhanced pinocytic capacity

Macrophage activation is very crucial for immune responses against invading pathogens. The enhancement of endocytosis, including phagocytosis and pinocytosis, is a distinguishing characteristic of macrophage activation (Yang et al., 2018; Zhan et al., 2020). Fig. 3B showed that SGP2-1 (40–320 μg/mL) remarkably increased neutral red uptake in RAW 264.7 macrophages. The result suggested that SGP2-1 could enhance the pinocytosis of RAW 264.7 macrophages.

3.6.3. SGP2-1 stimulated ROS generation

During phagocytosis, ROS generation helps in the eradication of invading pathogens (Lee et al., 2015). Additionally, ROS are essential second messengers to modulate signal transduction pathways in innate immune responses (West, Shadel, & Ghosh, 2011). To investigate whether SGP2-1 (40, 80, 160, and 320 μg/mL) treatment could stimulate ROS production, the DCFH-DA staining method was used to determine the intracellular ROS levels. Flow cytometry analysis suggested that, compared with the untreated cell, the mean fluorescence intensity of DCF was significantly increased in the SGP2-1 treated group (Fig. 3C). A similar result was found under fluorescence microscopy (Fig. 3D). These results indicated that the immunoregulation of SGP2-1 against invading pathogens in macrophages might be dependent on ROS generation.

3.6.4. SGP2-1 promoted inflammatory factors production and mRNA expression

Macrophages activated by immunomodulatory agents can promote the secretion of inflammatory factors, including NO and cytokines (TNF-α, IL-6, IL-10, MCP-1, etc.) (Liu, Chen, Chen, Huang, & Cheung, 2016). NO synthesized by iNOS is an indicator of macrophage activation. It is partly responsible for the killing of pathogenic microorganisms and tumor cells (Zhou et al., 2020). Fig. 4A showed that NO production was significantly increased in cells treated with SGP2-1 (40, 80, 160, and 320 μg/mL). Meanwhile, SGP2-1 treatment markedly up-regulated the mRNA levels of iNOS (Fig. 4E). These consistent results indicated that SGP2-1 promoted NO production through increasing the transcriptional levels of iNOS.

Apart from NO production, the secretion of cytokines such as TNF-α, IL-6, and MCP-1 by macrophages is also crucial for regulating the immune system. For instance, TNF-α can be involved in the defense against invading pathogens through improving the phagocytic functions of macrophages (Zhou et al., 2020). IL-6 functions as a critical cytokine in activating macrophages as well as a crucial signal molecule in altering the phenotype of macrophages. MCP-1 can regulate the migration and infiltration of macrophages (Liu et al., 2016). Thus, investigating the levels of TNF-α, IL-6 and MCP-1 is a good approach to examine the immunoregulatory activities of polysaccharides. As shown in Fig. 4B-D, SGP2-1 (40, 80, 160, and 320 μg/mL) treatment significantly promoted the secretion of TNF-α, IL-6, and MCP-1 compared with the control

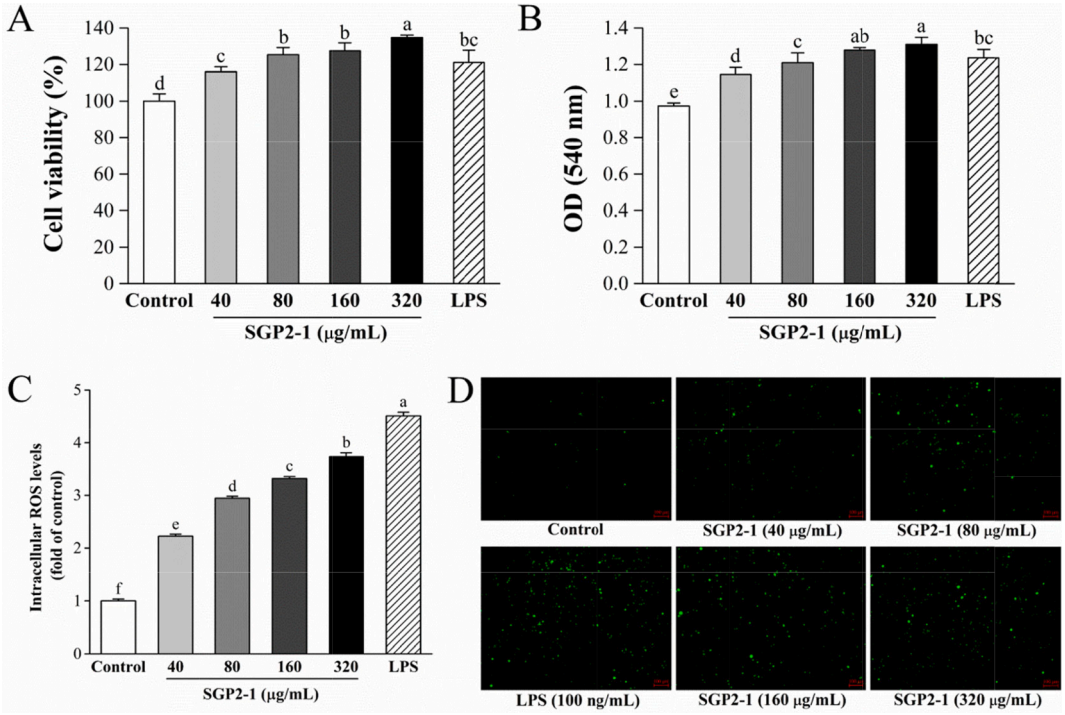

Fig. 3. Effect of SGP2-1 on the proliferation of RAW 264.7 cells (A); Effect of SGP2-1 on the pinocytic capacity of neutral red (B); Effect of SGP2-1 on ROS generation in RAW 264.7 cells analyzed by flow cytometry (C) and fluorescence microscope (D).

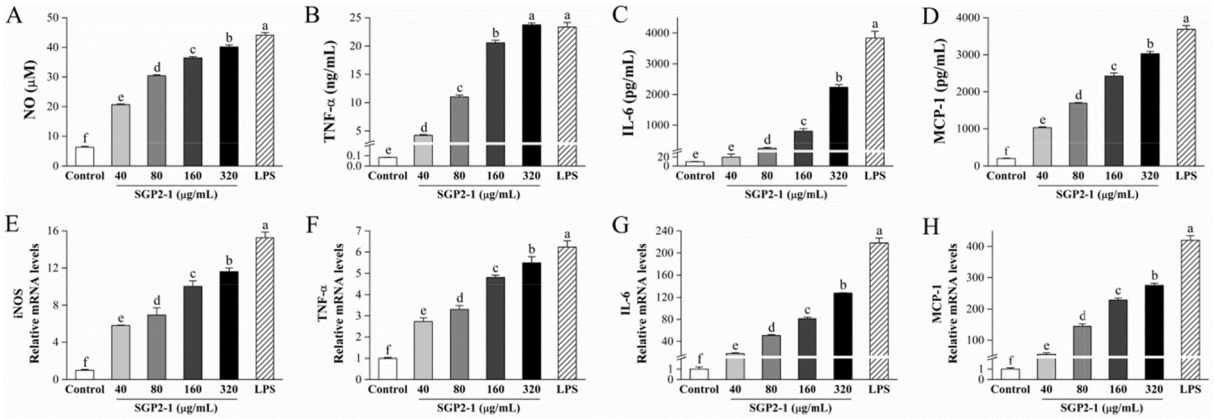

Fig. 4. Effects of SGP2-1 on the secretion of NO (A), TNF-α (B), IL-6 (C), and MCP-1 (D) in the cell culture supernatants and the mRNA expression of iNOS (E), TNF-α (F), IL-6 (G), and MCP-1 (H) in RAW 264.7 macrophages.

group. Moreover, the up-regulation of TNF-α, IL-6, and MCP-1 mRNA in RAW 264.7 cells were similar to the above results of cytokine production (Fig. 4F-H). These results suggested that SGP2-1 could elevate TNF-α, IL-6, and MCP-1 production by regulating gene transcription. During macrophage activation, the production of NO, TNF-α, and IL-6 are involved in M1 polarization, while the secretion of MCP-1 is found to be associated with M2 polarization (Liu et al., 2016; Liu et al., 2020). The above results suggested that SGP2-1 could cause an M1/M2 balance in macrophages.

3.6.5. *Recognition of SGP2-1 by TLR2*

Increasing evidence suggest that polysaccharides can exert immunomodulatory activities through binding to toll-like receptors of macrophages, such as TLR2 and TLR4 (Lee et al., 2015; Wu et al., 2017; Zhan et al., 2020). Therefore, whether TLR2 or TLR4 could be recognized by SGP2-1 to modulate macrophage activation was further investigated in this study. Compared with the group treated with SGP2-1 only, cells pretreated with TLR2 antibody remarkably reduced the secretion of NO and IL-6. However, no obvious change was found in the group treated with TLR4 antibody (Fig. S3). These results implied that TLR2 was involved in SGP2-1-mediated macrophage activation. Lee et al. (2015) found that polysaccharides from *Cordyceps militaris* culture broth induced TNF-α secretion in macrophages through TLR2, TLR4, and Dectin-1. Wu et al. (2017) reported that polysaccharides from *Hericium erinaceus* fruiting bodies were recognized by TLR2 and mannose receptors to exert immunostimulatory activity. These inconsistent results about the recognition of polysaccharides by receptors might be related to different structural characteristics. Several studies have demonstrated that polysaccharides structural features, including molecular weight, monosaccharide composition, glycosidic bonds, and degree of branching, are crucial for their immunostimulatory activity (Ferreira, Passos, Madureira, Vilanova, & Coimbra, 2015). A previous study indicated that (1 → 4)-α-glucans was recognized by TLR2 and exhibited immunomodulation in macrophages (Bittencourt et al., 2006). Several researches demonstrated that polysaccharides from *Ganoderma leucocontextum* (Gao et al., 2020), *Cordyceps sinensi* (Wang et al., 2017), and *Paecilomyces cicadae* (Ren et al., 2019) were mainly composed of → 4)-*α*-Glc*p*-(1 → residue and exhibited strong immunomodulatory activity. Therefore, the immunostimulatory activity of SGP2-1 might be partly attributed to its (1 → 4)-α-Glc*p* backbone structure.

3.3.6. *SGP2-1 activated mitogen-activated protein kinase (MAPKs), PI3K/Akt, and NF-κB signaling pathways*

MAPKs are a family of serine/threonine-specific protein kinases, including JNK, ERK, and p38. They have been proposed to participate in and control cellular response to the extracellular stimulus such as lipopolysaccharides, pro-inflammatory cytokines, and polysaccharides (Ren et al., 2017). Several researches have reported that polysaccharides from *Durvillaea Antarctica* (Yang et al., 2018), *Gynostemma pentaphyllum* (Ren et al., 2019), and *Isaria cicadae* (Xu et al., 2020) can activate macrophage through MAPKs phosphorylation. In the present study, whether MAPKs signaling pathway participated in SGP2-1-mediated RAW 264.7 macrophage activation was investigated. As presented in Fig. 5A, SGP2-1 (40, 80, 160, and 320 μg/mL) remarkably enhanced the phosphorylation of JNK, ERK, and p38. After treatment with 320 μg/mL of SGP2-1, the protein expression levels of p-JNK, p-ERK, and p-p38 were increased to 3.81, 5.95, and 6.88-fold, respectively. Moreover, specific inhibitors (SP600125, U0126, and SB203580) markedly reduced NO, TNF-α, and IL-6 secretion (Fig. 5D-E). These results indicated that SGP2-1 could stimulate macrophage through activating the MAPKs pathway.

PI3K signaling is crucial for proliferation, migration, survival, and growth in different types of cells. PIK3 and the downstream serine/threonine kinase Akt have recently attracted great attention due to their important functions in the immune system (Ren et al., 2017; Wu et al., 2017). Whether PI3K/Akt pathway participated in SGP2-1-mediated macrophage activation was investigated. Results showed that SGP2-1 treatment remarkably enhanced the phosphorylation of PI3K p85 and Akt compared with the control group. After treatment with 320 μg/mL of SGP2-1, the protein expression levels of p-PI3K p85 and p-Akt were increased to 1.51 and 2.50-fold, respectively (Fig. 5B). Moreover, the PI3K inhibitor LY294002 inhibited the stimulating effects of SGP2-1 on NO, TNF-α, and IL-6 production (Fig. 5D-E). These results implied that SGP2-1 activated RAW 264.7 cells was partly attributed to the regulation of PI3K/Akt pathway.

NF-κB is a crucial transcription factor. It can modulate mRNA transcription of various immune genes such as iNOS, TNF-α, and IL-6 (Ren et al., 2017; Zhan et al., 2020). Basically, NF-κB sequestered by IκB proteins exists as dimers in the cytoplasm in an unstimulated state. However, IκB proteins are phosphorylated and degraded through the ubiquitin–proteasome pathway under stimulation. Subsequently, released NF-κB migrates into the cell nucleus and regulates the transcription of target genes (Xu et al., 2020). It has been documented that the phosphorylation of MAPKs and Akt can mediate immunomodulatory effects through activating NF-κB transcription factor (Ren et al., 2019). Thus, whether SGP2-1 induced NF-κB activation was further explored. As can be seen from Fig. 5C, SGP2-1 (40, 80, 160, and 320 μg/mL) significantly enhanced the phosphorylation of NF-κB p65 and IκBα and decreased the protein expression level of IκBα. Additionally, SGP2-1 obviously promoted the translocation of NF-κB p65 into the nucleus. Furthermore, the NF-κB inhibitor BAY 11-7082 significantly reduced NO, TNF-α, and IL-6 secretion induced by SGP2-1 (Fig. 5D-E). Taken together, all these results suggested that SGP2-1-mediated cytokine secretion in macrophage was attributed to the activation of MAPKs, PI3K/Akt, and NF-κB pathways.

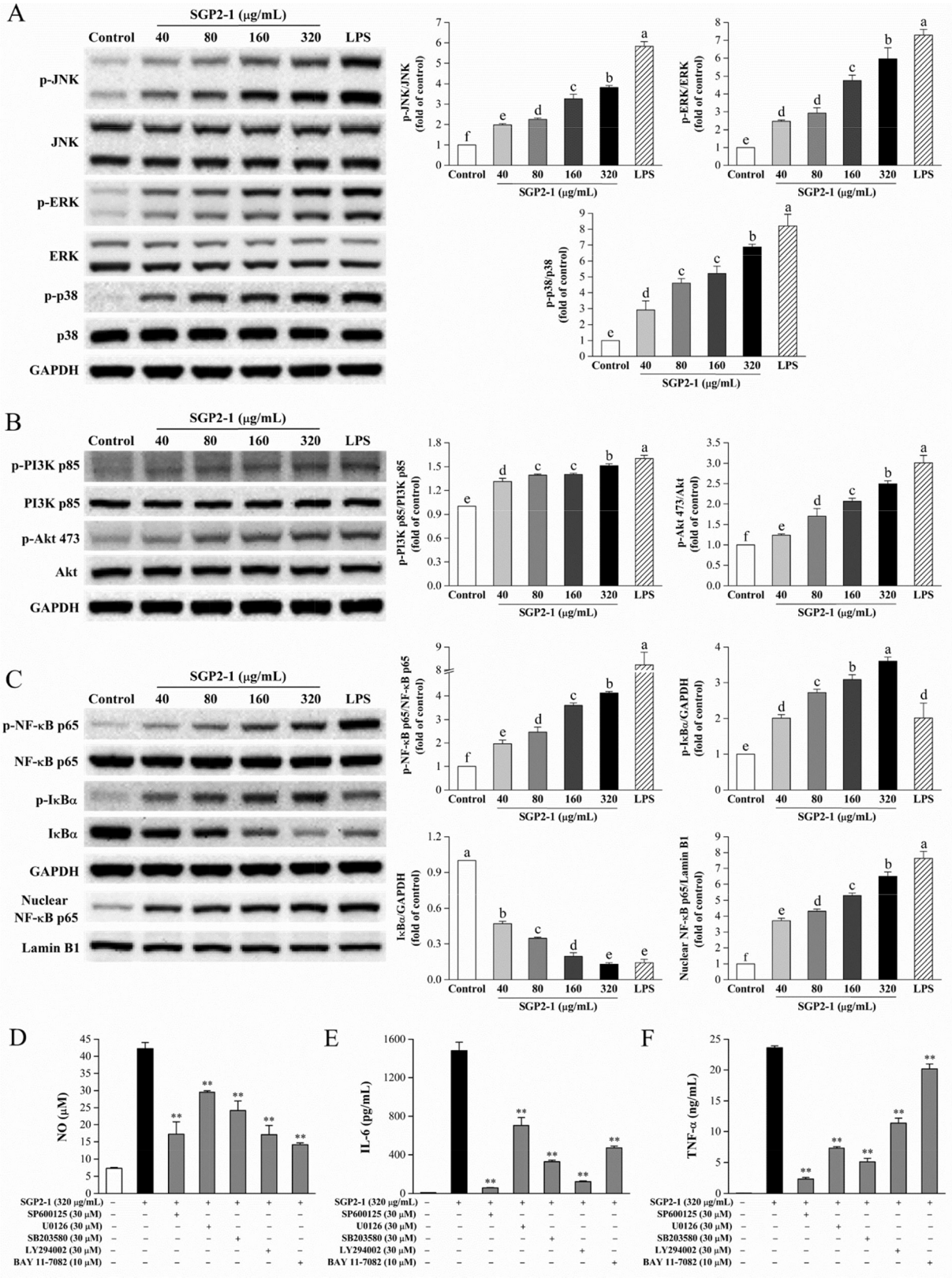

Fig. 5. Effects of SGP2-1 on MAPKs (A), PI3K/Akt (B), and NF-κB (C) signaling pathways in RAW 264.7 cells; Effects of SP600125, U0126, SB203580, LY294002, and BAY 11-7082 on NO (D), TNF-α (E), and IL-6 (F) secretion in RAW 264.7 cells induced by SGP2-1. $^{**}p < 0.01$ indicates significant difference from the group treated with SGP2-1 (320 μg/mL) only.

4. Conclusion

In this study, a new heteropolysaccharide, designated SGP2-1, was isolated from *S. granulatus* fruiting bodies. Its chemical structure was characterized by HPGPC, HPLC, FT-IR, GC–MS, and NMR. SGP2-1 with Mw of 150.75 kDa consisted of mannose, glucose, and xylose in a molar ratio of 7.6: 89.2: 3.2. It had a main backbone consisted of → 4)-*α*-Glc*p*-(1→, and the terminal group *α*-D-Glc*p* → was connected to the main chain by *O*-6 position. Moreover, SGP2-1 significantly promoted pinocytic capacity and ROS, NO, TNF-α, IL-6, and MCP-1 production in RAW 264.7 macrophages. SGP2-1 exerted immunostimulatory activity through recognizing TLR2 and activating MAPKs, PI3K/Akt, and NF-κB signaling pathways. Therefore, SGP2-1 could be developed as a potential functional food component for hypoimmunity and immunodeficiency diseases.

Declaration of Competing Interest

The authors declare that they have no known competing financial interests or personal relationships that could have appeared to influence the work reported in this paper.

Acknowledgments

This work was supported by the Funding of Introducing Innovation and Entrepreneurship Team Project in Zhaoqing High-tech Zone (2019ZHQ10), Guangdong Basic and Applied Basic Research Foundation (2019A1515110817), GDAS' Project of Science and Technology Development (2020GDASYL-202001033023), and Guangdong Province Agriculture Research Project and Agricultural Technique Promotion Project (2021KJ103).

Appendix A. Supplementary data

Supplementary data to this article can be found online at https://doi.org/10.1016/j.fochx.2022.100211.

References

Bittencourt, V. C. B., Figueiredo, R. T., Da Silva, R. B., Mourao-Sa, D. S., Fernandez, P. L., Sassaki, G. L., … Barreto-Bergter, E. (2006). An alpha-glucan of *Pseudallescheria boydii* is involved in fungal phagocytosis and toll-like receptor activation. *Journal of Biological Chemistry, 281*(32), 22614–22623. https://doi.org/10.1074/jbc.M511417200

Cao, C., Li, Y., Wang, C., Zhang, N., Zhu, X., Wu, R., & Wu, J. (2020). Purification, characterization and antitumor activity of an exopolysaccharide produced by *Bacillus velezensis* SN-1. *International Journal of Biological Macromolecules, 156*, 354–361. https://doi.org/10.1016/j.ijbiomac.2020.04.024

Chen, S., Su, T., & Wang, Z. (2018). Structural characterization, antioxidant activity, and immunological activity *in vitro* of polysaccharides from fruiting bodies of *Suillus granulatus*. *Journal of Food Biochemistry, 42*, e125153. https://doi.org/10.1111/jfbc.12515

Chen, W., Zhu, X., Ma, J., Zhang, M., & Wu, H. (2019). Structural elucidation of a novel pectin-polysaccharide from the petal of *Saussurea laniceps* and the mechanism of its anti-HBV activity. *Carbohydrate Polymers, 223*, 115077. https://doi.org/10.1016/j.carbpol.2019.115077

Cheng, Y., Xiao, X., Li, X., Song, D., Lu, Z., Wang, F., & Wang, Y. (2017). Characterization, antioxidant property and cytoprotection of exopolysaccharide-capped elemental selenium particles synthesized by *Bacillus paralicheniformis* SR14. *Carbohydrate Polymers, 178*, 18–26. https://doi.org/10.1016/j.carbpol.2017.08.124

Ferreira, S. S., Passos, C. P., Madureira, P., Vilanova, M., & Coimbra, M. A. (2015). Structure function relationships of immunostimulatory polysaccharides: A review. *Carbohydrate Polymers, 132*, 378–396. https://doi.org/10.1016/j.carbpol.2015.05.079

Gao, X., Qi, J., Ho, C., Li, B., Mu, J., Zhang, Y., … Xie, Y. (2020). Structural characterization and immunomodulatory activity of a water-soluble polysaccharide from *Ganoderma leucocontextum* fruiting bodies. *Carbohydrate Polymers, 249*, 116874. https://doi.org/10.1016/j.carbpol.2020.116874

Lee, J. S., Kwon, D. S., Lee, K. R., Park, J. M., Ha, S., & Hong, E. K. (2015). Mechanism of macrophage activation induced by polysaccharide from *Cordyceps militaris* culture broth. *Carbohydrate Polymers, 120*, 29–37. https://doi.org/10.1016/j.carbpol.2014.11.059

Lemieszek, M. K., Nunes, F. M., & Rzeski, W. (2019). Branched mannans from the mushroom *Cantharellus cibarius* enhance the anticancer activity of natural killer cells against human cancers of lung and colon. *Food & Function, 10*(9), 5816–5826. https://doi.org/10.1039/c9fo00510b

Li, Y., You, L., Dong, F., Yao, W., & Chen, J. (2020). Structural characterization, antiproliferative and immunoregulatory activities of a polysaccharide from Boletus *Leccinum rugosiceps*. *International Journal of Biological Macromolecules, 157*, 106–118. https://doi.org/10.1016/j.ijbiomac.2020.03.250

Liu, C., Chen, J., Chen, L., Huang, X., & Cheung, P. C. K. (2016). Immunomodulatory activity of polysaccharide-protein complex from the mushroom sclerotia of *Polyporus rhinocerus* in murine macrophages. *Journal of Agricultural and Food Chemistry, 64*(16), 3206–3214. https://doi.org/10.1021/acs.jafc.6b00932

Liu, C., Choi, M. W., Xue, X., & Cheung, P. C. K. (2019). Immunomodulatory effect of structurally characterized mushroom sclerotial polysaccharides isolated from *Polyporus rhinocerus* on bone marrow dendritic cells. *Journal of Agricultural and Food Chemistry, 67*(43), 12137–12143. https://doi.org/10.1021/acs.jafc.9b03294

Liu, H., Amakye, W. K., & Ren, J. (2021). *Codonopsis pilosula* polysaccharide in synergy with dacarbazine inhibits mouse melanoma by repolarizing M2-like tumor-associated macrophages into M1-like tumor-associated macrophages. *Biomedicine & Pharmacotherapy, 142*, 112016. https://doi.org/10.1016/j.biopha.2021.112016

Liu, W., Bi, S., Li, C., Zheng, H., Guo, Z., Luo, Y., … Yu, R. (2020). Purification and characterization of a new CRISP-related protein from *Scapharca broughtonii* and its immunomodulatory activity. *Marine Drugs, 18*, 2996. https://doi.org/10.3390/md18060299

Niu, Y., Shang, P., Chen, L., Zhang, H., Gong, L., Zhang, X., … Yu, L. L. (2014). Characterization of a novel alkali-soluble heteropolysaccharide from tetraploid *Gynostemma pentaphyllum* Makino and its potential anti-inflammatory and antioxidant properties. *Journal of Agricultural and Food Chemistry, 62*(17), 3783–3790. https://doi.org/10.1021/jf500438s

Reis, F. S., Stojkovic, D., Barros, L., Glamoclija, J., Ciric, A., Sokovic, M., … Ferreira, I. C. F. R. (2014). Can *Suillus granulatus* (L.) Roussel be classified as a functional food? *Food & Function, 5*(11), 2861–2869. https://doi.org/10.1039/c4fo00619d

Ren, D., Lin, D., Alim, A., Zheng, Q., & Yang, X. (2017). Chemical characterization of a novel polysaccharide ASKP-1 from *Artemisia sphaerocephala* Krasch seed and its macrophage activation via MAPK, PI3k/Akt and NF-kappa B signaling pathways in RAW264.7 cells. *Food & Function, 8*(3), 1299–1312. https://doi.org/10.1039/c6fo01699e

Ren, D., Zhao, Y., Zheng, Q., Alim, A., & Yang, X. (2019). Immunomodulatory effects of an acidic polysaccharide fraction from herbal *Gynostemma pentaphyllum* tea in RAW264.7 cells. *Food & Function, 10*(4), 2186–2197. https://doi.org/10.1039/c9fo00219g

Ren, J., Hou, C., Shi, C., Lin, Z., Liao, W., & Yuan, E. (2019). A polysaccharide isolated and purified from *Platycladus orientalis* (L.) Franco leaves, characterization, bioactivity and its regulation on macrophage polarization. *Carbohydrate Polymers, 213*, 276–285. https://doi.org/10.1016/j.carbpol.2019.03.003

Ren, L., Zhang, J., & Zhang, T. (2021). Immunomodulatory activities of polysaccharides from *Ganoderma* on immune effector cells. *Food Chemistry, 340*, 127933. https://doi.org/10.1016/j.foodchem.2020.127933

Ribeiro, B., Lopes, R., Andrade, P. B., Seabra, R. M., Goncalves, R. F., Baptista, P., … Valentao, P. (2008). Comparative study of phytochemicals and antioxidant potential of wild edible mushroom caps and stipes. *Food Chemistry, 110*(1), 47–56. https://doi.org/10.1016/j.foodchem.2008.01.054

Rungelrath, V., Kobayashi, S. D., & DeLeo, F. R. (2020). Neutrophils in innate immunity and systems biology-level approaches. *Wiley Interdisciplinary Reviews-Systems Biology and Medicine, 12*, e14581. https://doi.org/10.1002/wsbm.1458

Shi, W., Zhong, J., Zhang, Q., & Yan, C. (2020). Structural characterization and antineuroinflammatory activity of a novel heteropolysaccharide obtained from the fruits of *Alpinia oxyphylla*. *Carbohydrate Polymers, 229*, 115405. https://doi.org/10.1016/j.carbpol.2019.115405

Tabarsa, M., Dabaghian, E. H., You, S., Yelithao, K., Cao, R., Rezaei, M., … Bita, S. (2020). The activation of NF-kappa B and MAPKs signaling pathways of RAW264.7 murine macrophages and natural killer cells by fucoidan from *Nizamuddinia zanardinii*. *International Journal of Biological Macromolecules, 148*, 56–67. https://doi.org/10.1016/j.ijbiomac.2020.01.125

Teng, C., Qin, P., Shi, Z., Zhang, W., Yang, X., Yao, Y., & Ren, G. (2021). Structural characterization and antioxidant activity of alkali-extracted polysaccharides from quinoa. *Food Hydrocolloids, 113*, 106392. https://doi.org/10.1016/j.foodhyd.2020.106392

Wang, J., Nie, S., Cui, S. W., Wang, Z., Phillips, A. O., Phillips, G. O., … Xie, M. (2017). Structural characterization and immunostimulatory activity of a glucan from natural *Cordyceps sinensis*. *Food Hydrocolloids, 67*, 139–147. https://doi.org/10.1016/j.foodhyd.2017.01.010

Wang, Y., Yin, J., Huang, X., & Nie, S. (2020). Structural characteristics and rheological properties of high viscous glucan from fruit body of *Dictyophora rubrovolvata*. *Food Hydrocolloids, 101*, 105514. https://doi.org/10.1016/j.foodhyd.2019.105514

West, A. P., Shadel, G. S., & Ghosh, S. (2011). Mitochondria in innate immune responses. *Nature Reviews Immunology, 11*(6), 389–402. https://doi.org/10.1038/nri2975

Wu, F., Zhou, C., Zhou, D., Ou, S., & Huang, H. (2017). Structural characterization of a novel polysaccharide fraction from *Hericium erinaceus* and its signaling pathways involved in macrophage immunomodulatory activity. *Journal of Functional Foods, 37*, 574–585. https://doi.org/10.1016/j.jff.2017.08.030

Wu, F., & Huang, H. (2021). Surface morphology and protective effect of *Hericium erinaceus* polysaccharide on cyclophosphamide-induced immunosuppression in mice. *Carbohydrate Polymers, 251*, 116930. https://doi.org/10.1016/j.carbpol.2020.116930

Xie, X., Shen, W., Zhou, Y., Ma, L., Xu, D., Ding, J., … Zhou, C. (2020). Characterization of a polysaccharide from *Eupolyphaga sinensis* walker and its effective antitumor

activity via lymphocyte activation. *International Journal of Biological Macromolecules, 162*, 31–42. https://doi.org/10.1016/j.ijbiomac.2020.06.120

Xu, Z., Lin, R., Hou, X., Wu, J., Zhao, W., Ma, H., … Zhang, D. (2020). Immunomodulatory mechanism of a purified polysaccharide isolated from *Isaria cicadae* Miquel on RAW264.7 cells via activating TLR4-MAPK-NF-kappa B signaling pathway. *International Journal of Biological Macromolecules, 164*, 4329–4338. https://doi.org/10.1016/j.ijbiomac.2020.09.035

Yang, Y., Zhao, X., Li, J., Jiang, H., Shan, X., Wang, Y., … Yu, G. (2018). A beta-glucan from *Durvillaea Antarctica* has immunomodulatory effects on RAW264.7 macrophages via toll-like receptor 4. *Carbohydrate Polymers, 191*, 255–265. https://doi.org/10.1016/j.carbpol.2018.03.019

Yao, W., Chen, X., Li, X., Chang, S., Zhao, M., & You, L. (2021). Current trends in the anti-photoaging activities and mechanisms of dietary non-starch polysaccharides from natural resources. *Critical Reviews in Food Science and Nutrition*. https://doi.org/10.1080/10408398.2021.1939263

Yi, Y., Huang, X., Zhong, Z., Huang, F., Li, S., Wang, L., … Wang, H. (2019). Structural and biological properties of polysaccharides from lotus root. *International Journal of Biological Macromolecules, 130*, 454–461. https://doi.org/10.1016/j.ijbiomac.2019.02.146

Yu, Y., Zhang, Y., Hu, C., Zou, X., Lin, Y., Xia, Y., & You, L. (2019). Chemistry and immunostimulatory activity of a polysaccharide from *Undaria pinnatifida*. *Food and Chemical Toxicology, 128*, 119–128. https://doi.org/10.1016/j.fct.2019.03.042

Zhai, Z., Chen, A., Zhou, H., Zhang, D., Du, X., Liu, Q., … Su, P. (2021). Structural characterization and functional activity of an exopolysaccharide secreted by *Rhodopseudomonas palustris* GJ-22. *International Journal of Biological Macromolecules, 167*, 160–168. https://doi.org/10.1016/j.ijbiomac.2020.11.165

Zhan, Q., Wang, Q., Lin, R., He, P., Lai, F., Zhang, M., & Wu, H. (2020). Structural characterization and immunomodulatory activity of a novel acid polysaccharide isolated from the pulp of *Rosa laevigata* Michx fruit. *International Journal of Biological Macromolecules, 145*, 1080–1090. https://doi.org/10.1016/j.ijbiomac.2019.09.201

Zhao, X., Wei, Y., Gong, X., Xu, H., & Xin, G. (2020). Evaluation of umami taste components of mushroom (*Suillus granulatus*) of different grades prepared by different drying methods. *Food Science and Human Wellness, 9*(2), 192–198. https://doi.org/10.1016/j.fshw.2020.03.003

Zheng, X., Sun, H., Wu, L., Kong, X., Song, Q., & Zhu, Z. (2020). Structural characterization and inhibition on alpha-glucosidase of the polysaccharides from fruiting bodies and mycelia of *Pleurotus eryngii*. *International Journal of Biological Macromolecules, 156*, 1512–1519. https://doi.org/10.1016/j.ijbiomac.2019.11.199

Zhou, W., Zhao, Y., Yan, Y., Mi, J., Lu, L., Luo, Q., … Cao, Y. (2020). Antioxidant and immunomodulatory activities *in vitro* of polysaccharides from bee collected pollen of Chinese wolfberry. *International Journal of Biological Macromolecules, 163*, 190–199. https://doi.org/10.1016/j.ijbiomac.2020.06.244